This article has been accepted for publication in a future issue of this journal, but has not been fully edited. Content may change prior to final publication. Citation information: DOI 10.1109/TVT.2014.2351579, IEEE Transactions on Vehicular Technology

Shadow Fading Correlation in High-Speed Railway Environments

Ruisi He, *Member, IEEE*, Zhangdui Zhong, Bo Ai*, *Senior Member, IEEE* and Claude Oestges, *Senior Member, IEEE*

***Abstract*—In the design of diversity and fast handover schemes for high-speed railways (HSRs), a better understanding of the shadow fading correlation properties is required. In this paper, both auto- and cross-correlation models of shadow fading in HSR environments are proposed based on a large set of measurements with 6146 cells in China. The measurements are conducted using a practically deployed and operative GSM-Railway (GSM-R) system at 930 MHz, to reflect the real conditions of shadow fading in the HSR environments. 7 typical HSR environments and the realistic base station (BS) parameters are considered in the analysis. It is found that the decorrelation distance is correlated with the standard deviation of shadow fading, and is generally larger than 100 m in most of HSR environments. The cross-correlation of shadow fading between two neighboring BSs dependents on the BS height and the tilt angle of the antenna, and a heuristic truncated Gaussian distribution model of cross-correlation is proposed. The model is validated by the measurements conducted in another operative HSR line. The results can be used to exploit the simulation algorithms, to analyze the signal-to-interference-ratio (SIR) properties, and to develop new and better handover schemes for HSRs.**

***Index Terms*—Correlation, high-speed railways (HSRs), propagation, railway communications, shadow fading.**

I. Introduction

HIGH-SPEED railways (HSRs) are increasingly considered as a fast, safe and green transportation system. In China, the operative railway lines will be up to 120,000 km long by 2020, including over 16,000 km of HSR lines [3]. This also causes a dramatic increase in HSR communications, so that additional techniques are required to enhance the performance of the GSM-Railway (GSM-R) based control system. Among the many challenges faced when designing a safe and reliable GSM-R network for HSR, handover is prevalent because of the high handover frequency. A deep understanding of shadowing fading is thus required to design and test improved handover algorithms, slow power control, and network planning [4]–[6]. The impact of shadow fading on handover performance is of particular interest, as the handover performance has been found to be sensitive to the standard deviation and correlation properties of shadow fading. The fluctuations of signal strength associated with shadow fading cause a call sometimes to be repeatedly handed over back and forth between neighboring base stations (BSs), which is mostly called the "ping-ponging" effect [7]. In [8], it is observed that the handover rate and handover initiation delay increases and decreases with the standard deviation of shadow fading, respectively. The effect of the hysteresis margin on handover performance is also found to depend on its relative value in terms of the standard deviation of shadow fading in [8]. In [9], the lognormally distributed shadow fading component is used for the simulation of handover scheme performance in HSR environments, however, the correlation properties of shadow fading are not considered in [9].

It has also been claimed that the handover performance is sensitive to the correlation properties of shadow fading. In [10], a least squares estimate of path-loss parameters of the various radio links is proposed based on the auto-correlation model of shadow fading, and is found to have better performance than the handover algorithm based on averaging the signal strength [11]. In [12], the simulation shows that the call dropping performance of a wireless network displays a "resonance"-like behavior, i.e. the call dropping curve peaks at a critical correlation length of shadow fading. It is thus critical to capture spatial auto-correlation of shadow fading when studying the performance of wireless network. In [13], the cross-correlation is found to determine an increase of probability of handover with respect to the case of non-cross-correlated shadowing, and significant variations are observed in both the number of handovers and handover delay due to the presence of cross-correlation. In [14], an improved location-based handover algorithm is proposed, which exploits the auto- and cross-correlation properties of shadow fading to avoid unnecessary handovers.

In addition, characterizing shadow fading correlation is useful in the analysis of macrodiversity and system design, e.g., the decorrelation distance dictates how rapidly the large-scale signal-to-noise ration (SNR) changes, whereas the cross-correlation significantly affects the gain achieved by macroscopic diversity. Moreover, the effects of shadow fading correlation must be accounted for in order to decrease the difference between simulation results and experimental deployment results.

Part of the work is presented in 2014 IEEE International Symposium on Antennas and Propagation [1] and 2014 URSI General Assembly and Scientific Symposium [2]. The work is supported by the Key Grant Project of Chinese Ministry of Education (No.313006), the National Natural Science Foundation of China under Grant 61222105 and U1334202, the National 863 Project under Grant 2014AA01A706, the Fundamental Research Funds for the Central Universities under Grant 2014JBZ021, and the Key Project of the State Key Lab of Rail Traffic Control and Safety under Grant RCS2012ZT013, RCS2014ZZ03, and RCS2014ZT32.

R. He, Z. Zhong, and B. Ai* (correspondence author) are with the State Key Laboratory of Rail Traffic Control and Safety, Beijing Jiaotong University, Beijing 100044, China (e-mail: ruisi.he@ieee.org, zhdzhong@bjtu.edu.cn, boai@bjtu.edu.cn).

C. Oestges is with the Institute for Information and Communication Technologies, Electronics and Applied Mathematics, Université catholique de Louvain, 1348 Louvain-la-Neuve, Belgium (e-mail: claude.oestges@uclouvain.be).

This article has been accepted for publication in a future issue of this journal, but has not been fully edited. Content may change prior to final publication. Citation information: DOI 10.1109/TVT.2014.2351579, IEEE Transactions on Vehicular Technology

TABLE I
SUMMARY OF INVESTIGATION ON SHADOW FADING IN HSR ENVIRONMENTS

Reference	Frequency	Scenario	Using high-speed train	Shadow fading distribution	Shadow fading auto-correlation	Shadow fading cross-correlation
[1]	930 MHz	Urban	√	×	√	×
[1]	930 MHz	Suburban	√	×	√	×
[1]	930 MHz	Rural	√	×	√	×
[2]	930 MHz	Viaduct	√	×	×	√
[15]	5.2 GHz	Rural	×	√	×	×
[16]	930 MHz	Viaduct	√	√	√	×
[17]	2.35 GHz	Viaduct	√	√	√	×
[18]	930 MHz	Viaduct	√	√	×	×
[19]	2.35 MHz	Viaduct	√	√	×	×
[20]	2.35 GHz	Viaduct	√	√	×	×
[21]	2.6 GHz	Viaduct	√	√	×	×
[22]	930 MHz	Cutting	√	√	×	×
[23]	2.35 GHz	Cutting	√	√	×	×
[24]	2.4 GHz	Hilly	√	√	×	×
[25]	400 MHz	Rural	×	×	×	×

Subsequent to the above analysis, a shadow fading model for HSRs is required to tackle the following issues: i) an auto-correlation model and the prediction of decorrelation distance; ii) a cross-correlation model for two neighboring BSs. To this end, a large set of measurements is required. Therefore, we carried out an extensive measurement campaign, with 6146 cells, along Chinese HSR lines. In this paper, we extend our previous work [1], [2] to 7 typical HSR environments: urban, suburban, rural, viaduct, cutting, station, and river. For each environment, the shadow fading behavior is analyzed, auto- and cross-correlation models are proposed, implemented and validated.

The paper is organized as follows: Section II summaries the related work about shadow fading correlation. Section III introduces the measurement system and environments. Section IV outlines the basic theory of shadow fading. Section V presents the shadow fading models, and the implementation and validation of models. Finally, Section VI concludes the paper.

II. RELATED WORK

In the past decades, HSR radio channel modeling has attracted much interest due to the high demand for GSM-R network planning. In our previous work, the auto-correlation characteristics in urban, suburban, and rural were analyzed [1], and the cross-correlation characteristics in the viaduct environment were investigated [2], both at 930 MHz. In the WINNER II model [15], the shadowing standard deviation in rural environments was analyzed, however, it did not rely on using high-speed trains for the measurements. In [16], the auto-correlation of shadow fading in an HSR viaduct scenario was investigated and the double exponential model was suggested to describe the shadow fading auto-correlation. In [17], the shadowing correlation and the cross-correlation between shadow fading and delay spread were investigated in HSR viaduct environments at 2.35 GHz. In [18]–[21], the standard deviation of shadow fading in HSR viaduct environments was analyzed at 930 MHz, 2.35 GHz, and 2.6 GHz, respectively. In [22], [23], the standard deviation of shadow fading in HSR cutting environments was analyzed at 930 MHz and 2.35 GHz, respectively, and the impact of structure of cutting on shadow fading was modeled. In [26], cutting in HSRs was considered as an open area and the shadow fading was analyzed. The impact of overbridges on shadow fading was discussed, though without any realistic measurements in [26]. In [24], HSR channel measurements were conducted in hilly terrains at 2.4 GHz and shadow fading distribution was compared with viaduct measurements. In [25], a train-to-train channel model was developed at 400 MHz for train collision avoidance and shadow fading was analyzed. Finally, some recent measurements investigated the delay and Doppler characteristics in HSR environments. As those those do not deal with shadow fading, we do not detail them here, but invite the reader refer to [27], [28], and the references therein.

In Table I, we summarize and classify the existing measurement campaigns about shadow fading in HSR environments, according to frequency, scenario, whether using the high-speed train in the measurements, and which issues of shadow fading are addressed. We can see that most works focus on the viaduct scenario and that the correlation properties, e.g., the auto- and cross-correlation behaviors, are largely neglected.

Naturally, some results exist as far as cellular channels are concerned. While these works might not be readily scalable to HSR environments (because those results are based on measurements either outside the GSM-R frequency band or in non-railway environments), they provide some insight into the correlation properties of shadow fading. For example, in [29]–[31], an exponential model was suggested to describe the auto-correlation function of shadow fading in suburban and urban environments, which is consistent with the HSR measurements in [17]. In [6], [32]–[36], the cross-correlation of shadow

This article has been accepted for publication in a future issue of this journal, but has not been fully edited. Content may change prior to final publication. Citation information: DOI 10.1109/TVT.2014.2351579, IEEE Transactions on Vehicular Technology

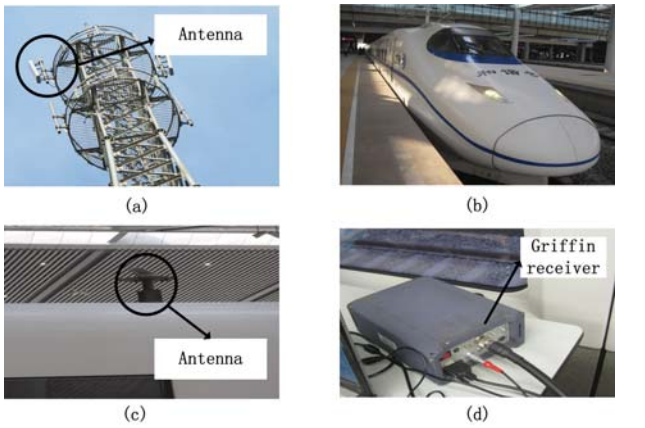

Fig. 1. Measurement system. (a) Base station and APX86-906515S-CT0 TX antenna, mounted with a tilt angle against the tower. (b) High-speed train in the measurements. (c) 900/2400-HBNT RX antenna, placed on the roof of the train. (d) Willtek 8300 Griffin receiver.

fading was experimentally characterized and models were proposed based on the distance and/or the angle difference between the links. In HSRs, as the BSs are located along the linear rail track, the distance and angle differences are mostly affected by the BS height and tilt angle (as detailed in Section IV).

III. Measurements

A. Measurement Campaign

We conducted an extensive measurement campaign along the "Zhengzhou-Xian" HSR lines of China at 930 MHz. A practically deployed and operative GSM-R system was used. The GSM-R BSs were placed along the HSR line, generally 10 m away from the rail track. The BS antennas were 20-40 m higher than the surface of the rail track so that our measurements were generally conducted in line-of-sight (LOS) conditions. Fig. 1 depicts the measurement system (more details of the system can be found in [37]–[39]). To record sufficient data, we conducted repeated measurements for over one year and measured 6146 HSR cells. We used a distance sensor to trigger the system and ensure that the spatial sampling interval was fixed at 53 cm, irrespective of the train speed. Using the sweeping mode of a Willtek 8300 Griffin receiver, the received power was measured from both neighboring BSs. The difference of frequency for two neighboring BSs was 12 MHz. Since GSM-R has a bandwidth of 0.2 MHz, the interference between two neighboring BSs is thus negligible. The average SNR was generally larger than 30 dB, so that an accurate estimation of channel parameters is possible.

B. Environment

Radio propagation depends on topographical and electromagnetic features of the operating environment. A propagation scene partitioning for HSR scenarios was first proposed in [40], where HSR environments are divided into 19 environments. We selected 7 most typical HSR environments to conduct our measurements. Brief descriptions are as follows[1]:

[1]A detailed description of each environment can be found in [41].

Fig. 2. Railway-specific environments. (a) Left to right: urban, suburban and rural. (b) Viaduct. (c) Cutting, from [38]. (d) Railway station with large awnings on top, from [40]. (e) River.

TABLE II
Cell Number of each Railway Environment in the Measurements

Environment	Number
Urban	66
Suburban	1500
Rural	808
Viaduct	2114
Cutting	638
Station	772
River	248

1) *Urban*: large and densely built cities with most buildings over 10 floors.
2) *Suburban*: low residential or townhouses with one or few floors; a few trees.
3) *Rural*: mostly open areas, with very few buildings along the track.
4) *Viaduct*: viaduct with heights ranging from 10 m to 30 m [37].
5) *Cutting*: cuttings with steep walls on both sides [38].
6) *Station*: regular railway cell with one railway station (usually with awnings on top) at the beginning or end of the cell (awning is usually 0.4-0.8 km long, 0.1-0.5 km wide, and 50-80 m high; BSs are mostly located outside the awnings).
7) *River*: rivers (usually 50-200 m wide) either on one side of the track, or crossing the rail line.

Fig. 2 illustrates these railway-specific environments. Table II summarizes the number of cells used in the measurements for each environment. Generally, over hundreds of cells are used to ensure the accuracy of analysis.

This article has been accepted for publication in a future issue of this journal, but has not been fully edited. Content may change prior to final publication. Citation information: DOI 10.1109/TVT.2014.2351579, IEEE Transactions on Vehicular Technology

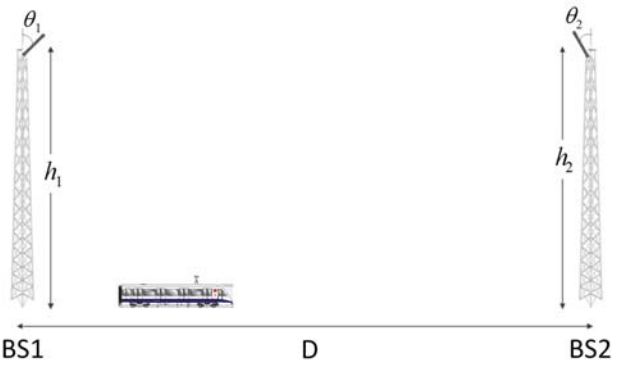

Fig. 3. Sketch map of two neighboring BSs.

TABLE III
PASSING RATE OF THE GAUSSIAN DISTRIBUTION AND STANDARD DEVIATION (STD) OF SHADOW FADING IN RAILWAY ENVIRONMENTS

Environment	KS Passing Rate (%)	Mean STD, σ (dB)
Urban	96.97	3.19
Suburban	85.48	3.33
Rural	93.61	2.85
Viaduct	91.92	2.73
Cutting	91.60	3.63
Station	84.59	2.77
River	91.09	3.09

IV. SHADOW FADING MODEL

Fig. 3 shows a sketch map of two BSs and one high-speed train. For convenience, we name the pair of BSs in Fig. 3 the neighboring cells (NCs). Each BS in a NC has two parameters: the antenna height h over the rail track surface and the tilt angle θ against the BS tower. Parameter D is the separation distance between the two BSs. We denote as r_1 and r_2 the local measured mean power of the signals received from BS1 and BS2, i.e., transmitter 1 (TX1) and transmitter 2 (TX2), respectively. The mean power values are obtained after averaging the instantaneous received power over a 40-wavelength sliding (non-overlapping) window. Both r_1 and r_2 can be modeled as [42]

$$r_s(d_s) = A_s + 10n_s\log_{10}(d_s) + X_s \ , \tag{1}$$

where $s = 1, 2$ denote the TX1-RX and TX2-RX links, respectively; A_s is the intercept value and n_s is the path loss exponent, both of which are obtained by using a Least Square (LS) regression fit; d_s is the TX-RX separation distance; X_s denotes the shadow fading component.

The shadowing fluctuation (in decibels) is usually characterized by a zero-mean Gaussian distribution,

$$X_s \sim N[0, \sigma_s] \ , \tag{2}$$

where $N[0, \sigma_s]$ represents a Gaussian distribution with zero mean and a standard deviation of σ_s.

To analyze the correlation characteristics, the auto- and cross-correlation coefficients are estimated from the shadowing samples as follows:

- the auto-correlation coefficient estimate for a given TX-RX link is defined as in Eq. (3), where N is the number of the samples; Δd represents the distance difference; $\overline{(\cdot)}$ denotes the sample mean value of the set $(\cdot)$.
- the cross-correlation coefficient between the TX1-RX and TX2-RX links is estimated as

$$\hat{\rho}_{\text{cross}} = \frac{\sum_{i=1}^{N}\left(X_{1,i} - \overline{X_1}\right)\left(X_{2,i} - \overline{X_2}\right)}{\sqrt{\sum_{i=1}^{N}\left(X_{1,i} - \overline{X_1}\right)^2} \cdot \sqrt{\sum_{i=1}^{N}\left(X_{2,i} - \overline{X_2}\right)^2}}. \tag{4}$$

To increase the reliability of the analysis, the confidence interval (CI) of the estimated correlation coefficients $\hat{\rho}$ is analyzed based on the Fisher z-transformation [43]. The transformation is defined by

$$z = \frac{1}{2}\log_e\left(\frac{1+\hat{\rho}}{1-\hat{\rho}}\right) \ . \tag{5}$$

For a given significance level α, i.e., the CI is $1-\alpha$, the lower and upper limits are expressed as [44]

$$\left[\frac{\exp(2z_1)-1}{\exp(2z_1)+1} \quad \frac{\exp(2z_2)-1}{\exp(2z_2)+1}\right] \ , \tag{6}$$

where

$$z_1 = z - \left(\frac{\Phi_{1-\alpha/2}}{\sqrt{N-3}}\right), \quad z_2 = z + \left(\frac{\Phi_{1-\alpha/2}}{\sqrt{N-3}}\right) \ , \tag{7}$$

and $\Phi_{1-\alpha/2}$ is the appropriate value from the standard Gaussian distribution for the $1-\alpha$ percentile, which can be found in [45]. In the following, the 95% CIs of the estimated correlation coefficients are used.

V. RESULTS

A. Shadow Fading Standard Deviation

Our measurements suggest that the zero-mean Gaussian distribution fits the shadowing data (in dB) in each environment. We use the Kolmogorov-Smirnov (KS) test with a CI of 95% to validate this assumption. The statistic of the KS test is defined as the maximum value of the absolute difference between the cumulative distribution function (CDF) of the measured shadow fading components Y_1 and the CDF of the estimated distribution Y_2, which can be expressed as

$$\mathrm{D_{KS}} = \max\left(|F(Y_1) - F(Y_2)|\right) \ , \tag{8}$$

where $F(\cdot)$ denotes the CDF of $(\cdot)$. $|(\cdot)|$ denotes the absolute value of $(\cdot)$. To test the goodness of fit, the KS test compares $\mathrm{D_{KS}}$ to a threshold $\mathrm{D_{th}}$ corresponding to a given significance level α. In our analysis, $\alpha = 5\%$, i.e., the CI is 95%. Therefore, we have $\mathrm{D_{th}} = 1.36/\sqrt{N}$ [46]. Any distribution for which $\mathrm{D_{KS}} > \mathrm{D_{th}}$, is rejected with significance 95%, while any distribution for which $\mathrm{D_{KS}} \leq \mathrm{D_{th}}$ is accepted with the same level of significance. Table III summarizes the KS passing rate of the zero-mean Gaussian distribution in each environment. It is found that the KS passing rate is larger than 84% in all environments.

This article has been accepted for publication in a future issue of this journal, but has not been fully edited. Content may change prior to final publication. Citation information: DOI 10.1109/TVT.2014.2351579, IEEE Transactions on Vehicular Technology

$$\hat{\rho}_{\text{auto}}(\Delta d) = \frac{\sum_{i=1}^{N} \left(X_s(d_{s,i}) - \overline{X_s(d_s)} \right) \cdot \left(X_s(d_{s,i} + \Delta d) - \overline{X_s(d_s + \Delta d)} \right)}{\sqrt{\sum_{i=1}^{N} \left(X_s(d_{s,i}) - \overline{X_s(d_s)} \right)^2} \cdot \sqrt{\sum_{i=1}^{N} \left(X_s(d_{s,i} + \Delta d) - \overline{X_s(d_s + \Delta d)} \right)^2}} \tag{3}$$

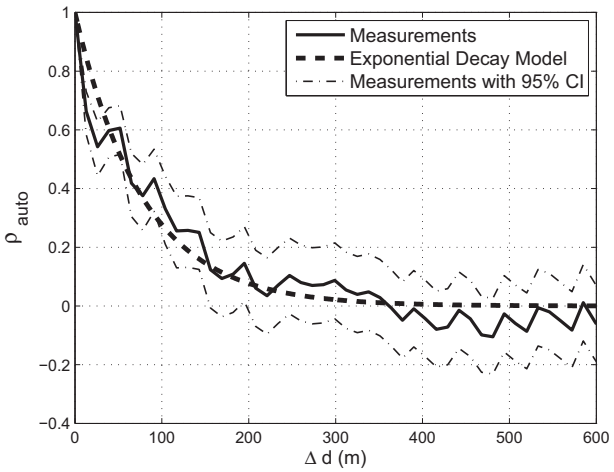

Fig. 4. Example plot of the measured $\hat{\rho}_{\text{auto}}(\Delta d)$ in one cell of the viaduct environments, together with an exponential decay model.

The mean value of the standard deviation of shadowing in each environment is also presented in Table III: it ranges from 2.7 to 3.7 dB. We also note that σ is significantly less in HSR scenarios than in classical cellular systems, e.g., in [31], σ is larger than 7 dB in urban areas, in [47], $\sigma = 8.2$ dB in suburban areas, and in [48], σ is large than 6 dB in urban and rural areas. This is because in HSR networks, the high BS leads to clear LOS propagation with reduced shadowing effects.

B. Shadowing Auto-Correlation Characteristics

For the measurements from each BS in Fig. 3 (in a particular scenario), we estimate the auto-correlation coefficient $\hat{\rho}_{\text{auto}}$ from (3). In our measurements $\hat{\rho}_{\text{auto}}$ has been found to follow an exponential decay function [29], expressed as

$$\hat{\rho}_{\text{auto},j}(\Delta d) = \exp\left(-\frac{\Delta d}{d_{\text{cor},j}} \right) , \tag{9}$$

where j is the index of the specific railway environment; d_{cor} represents the decorrelation distance, which depends on the scenario and is usually defined to be the distance at which the correlation drops to $1/e$. The decorrelation distance reflects how fast the large-scale parameters are changing over the route. Example plot of the measured $\hat{\rho}_{\text{auto}}$ in viaduct environments is shown in Fig. 4, where we can see that the exponential decay function offers a good fit to the measurements. Note that Eq. (9) ranges between 0 and 1, and can not reflect the negative $\hat{\rho}_{\text{auto}}$, as in Fig. 4. However, the estimated $\hat{\rho}_{\text{auto}}$ drops below 0 only for large Δd (three times of d_{cor}). In that range, the variation of $|\hat{\rho}_{\text{auto}}|$ is at most 0.2. Therefore, we still use the classical exponential decay model of Eq. (9) in this paper.

TABLE IV
SHADOWING AUTO-CORRELATION ANALYSIS

Environment	Mean, d_{cor} (m)	$\hat{\Gamma}_j$, [95% CI]
Urban	57.12	0.28, [0.04 0.49]
Suburban	112.48	0.38, [0.34 0.42]
Rural	114.79	0.25, [0.18 0.32]
Viaduct	115.44	0.23, [0.19 0.27]
Cutting	88.78	0.34, [0.28 0.39]
Station	101.22	0.42, [0.36 0.48]
River	114.58	0.19, [0.07 0.31]

In Fig. 4, the various measurement curves are plotted together with with the 95% CI estimated for each particular $\hat{\rho}_{\text{auto}}(\Delta d)$ from Eq. (5)-(7). We can see that the CI is reasonably narrow before $\hat{\rho}_{\text{auto}}$ drops to 0.2, which shows that the estimation of d_{cor} with $1/e$ threshold has sufficient accuracy. Note that the CI tightness depends on the number of samples. As we use a 40-wavelength sliding non-overlapping window to remove small-scale fading effects, in each cell the number of shadow fading samples is less than 300, which limits the CI tightness.

For the estimated distance d_{cor} in each environment, we examine the dependency of d_{cor} on the scenario parameters: h, θ, D and h/θ, as in Fig. 3. As we find that d_{cor} is independent of those parameters, we directly model the mean value of d_{cor} for each railway environment (see Table IV). We observe that in most railway environments, d_{cor} is larger than 100 m; only in the urban and cutting environments, values less than 90 m are observed. We conjecture that it is caused by the rich reflection/scattering components in urban and cutting environments. This result is consistent with the results in [15] and [34], where $d_{\text{cor}} \leq 90$ m is suggested for LOS urban areas.

Furthermore, we note that, in each cell, a higher shadow fading standard deviation σ usually corresponds to a larger value of d_{cor}, as shown in Fig. 5. It is conjectured that the scatterers that increase the decorrelation distance usually lead to a larger variation of shadow fading. We therefore derive a correlation coefficient $\hat{\Gamma}_j$ in the j-th environment, expressed as

$$\hat{\Gamma}_j = \frac{\sum_{i=1}^{N} \left(\sigma(i) - \overline{\sigma} \right) \left(d_{\text{cor}}(i) - \overline{d_{\text{cor}}} \right)}{\sqrt{\sum_{i=1}^{N} \left(\sigma(i) - \overline{\sigma} \right)^2} \cdot \sqrt{\sum_{i=1}^{N} \left(d_{\text{cor}}(i) - \overline{d_{\text{cor}}} \right)^2}} . \tag{10}$$

The coefficient $\hat{\Gamma}_j$ is summarized in Table IV, together with the 95% CIs estimated from Eq. (5)-(7). The values of CIs

This article has been accepted for publication in a future issue of this journal, but has not been fully edited. Content may change prior to final publication. Citation information: DOI 10.1109/TVT.2014.2351579, IEEE Transactions on Vehicular Technology

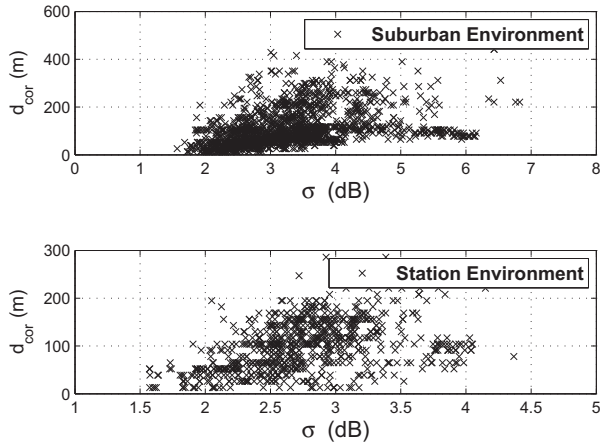

Fig. 5. Example plots of $d_{\rm cor}$ vs σ in suburban and station environments.

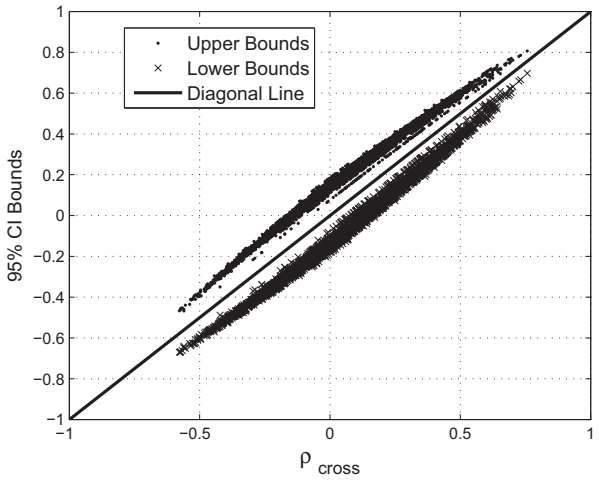

Fig. 6. Example plots of the 95% CI bounds of $\hat{\rho}_{\rm cross}$ in all environments. Diagonal line is plotted for reference.

indicate a reasonable estimation accuracy, because of the large data set in Table II. Generally, $\hat{\Gamma}_j$ is larger than 0.2, and its positiveness confirms that larger σ values are associated with larger $d_{\rm cor}$.

C. Shadowing Cross-Correlation Characteristics

For each NC (in a particular scenario) as in Fig. 3, we estimate the cross-correlation coefficient by (4). The 95% CIs of the estimated $\hat{\rho}_{\rm cross}$ are plotted in Fig. 6, using Eq. (5)-(7). The estimated CIs in Fig. 6 are limited by the number of shadowing samples in each cell, as discussed before. It is found that the 95% CI is reasonably narrow. A relatively wide CI is only observed for a small value of $|\hat{\rho}_{\rm cross}|$.

1) *Discussions*: It is found that the cross-correlation coefficient $\hat{\rho}_{\rm cross}$ exhibits a large fluctuation from cell to cell. It is conjectured that $\hat{\rho}_{\rm cross}$ is affected by factors such as antennas, BSs, environments, etc. We thus examine some of these factors in the following and then propose a heuristic model for $\hat{\rho}_{\rm cross}$.

Several factors are considered: the environment where the NC is located; the separation distance D between the two BSs; the heights h of the two BSs; and the tilt angles θ of the antennas against the BS towers:

- Environment: It has been found in [37], [38] that the environment type significantly affects the large- and small-scale characteristics. The same is observed for $\rho_{\rm cross}$. Therefore, we distinguish different environments when we model $\hat{\rho}_{\rm cross}$. As shown in Table II, we have sufficient measurements in each environment to ensure an accurate analysis.
- Separation distance D: A dependency of $\hat{\rho}_{\rm cross}$ on D is not observed in our measurements. One possible reason is that D in our measurements is always around 3-4 km, which does not cover a sufficiently large range. We also note that, as reported in [35], a clear dependency of cross-correlation can only be observed when TX/RX separation distance is around 1000 m, which is not a realistic case for HSR deployment. Since we use the operative GSM-R network in the measurements, changing D to have more realizations is not feasible in our current work. We therefore do not consider the impact of D on $\hat{\rho}_{\rm cross}$ in the following model.
- h and θ: As indicated in [49], [50], for a particular antenna gain pattern, the BS antenna height h and angle θ determine the gain and the received power at different locations. A large h or a small θ usually lead to better coverage for most of the railway cell. We therefore introduce a heuristic term of h/θ to represent the impact of BS on the cross-correlation characteristics[2]. The difference of h/θ between the two BSs can be expressed as

$$\xi = \left| \frac{h_1}{\theta_1} - \frac{h_2}{\theta_2} \right| . \tag{11}$$

A small ξ means that the two neighboring BSs generally have similar impacts on the shadow fading of the two TX-RX links, i.e., a large $|\hat{\rho}_{\rm cross}|$ is expected. In Table V, we summarize the number of measured $\hat{\rho}_{\rm cross}$ for each realization of ξ in the measurements. We observe that except for urban areas, sufficient realizations enable to examine the dependency of $\hat{\rho}_{\rm cross}$ on ξ, and that for each realization of ξ, we generally have sufficient samples of $\hat{\rho}_{\rm cross}$ to ensure an accurate analysis.

2) *Notation*: Before proposing the model, we define the following notations:

- $\xi_{j,q}$ denotes the q-th realization of ξ in the j-th scenario, where $q = 1, 2, \cdots, Q_j$ and Q_j is the total number of realization ξ in the j-th scenario.
- $\Phi_{j,q}$ denotes a set of cross-correlation coefficients, which correspond to the NCs with a realization of $\xi_{j,q}$ in the j-th scenario.
- $\hat{\rho}_{{\rm cross},j,q,p}$ denotes the p-th cross-correlation coefficient in the set $\Phi_{j,q}$, where $p = 1, 2, \cdots, P_{j,q}$ and $P_{j,q}$ is the total number of cross-correlation coefficients in the set $\Phi_{j,q}$.

3) *Model*: Example plots of $\rho_{\rm cross}$ values measured in the viaduct and cutting environments are shown in Fig. 7. Our first

[2]Other terms like $h/\tan(\theta)$ were also examined. However, the term h/θ offers the best fit to the data.

This article has been accepted for publication in a future issue of this journal, but has not been fully edited. Content may change prior to final publication. Citation information: DOI 10.1109/TVT.2014.2351579, IEEE Transactions on Vehicular Technology

TABLE V
NUMBER OF MEASURED $\hat{\rho}_{\text{cross}}$ VALUES FOR EACH REALIZATION OF ξ IN THE MEASUREMENTS

Environment	Realizations of ξ	Number of $\hat{\rho}_{\text{cross}}$ for each realization of ξ
Urban	(1.6)	(33)
Suburban	(0, 0.71, 1.25, 1.42, 1.43, 1.71, 1.96, 2.29, 2.46, 2.86, 3.39, 5.71)	(355, 18, 95, 24, 26, 26, 25, 78, 26, 26, 26, 25)
Rural	(0, 0.40, 0.71, 1.25, 2.14, 4.25, 11.79)	(78. 107, 26, 26, 26, 35, 106)
Viaduct	(0, 0.15, 0.71, 1.25, 1.75, 2.46, 2.50, 3.00)	(524, 16, 30, 193, 103, 59, 26, 106)
Cutting	(0, 0.71, 1.04, 1.25, 1.43, 1.86, 3.54)	(93, 24, 26, 104, 52, 20, 181)
Station	(0, 0.86, 3.04, 3.54, 4.25, 5.18, 6.21)	(50, 3, 14, 100, 109, 26, 84)
River	(0, 1.5, 2.5)	(74, 24, 26)

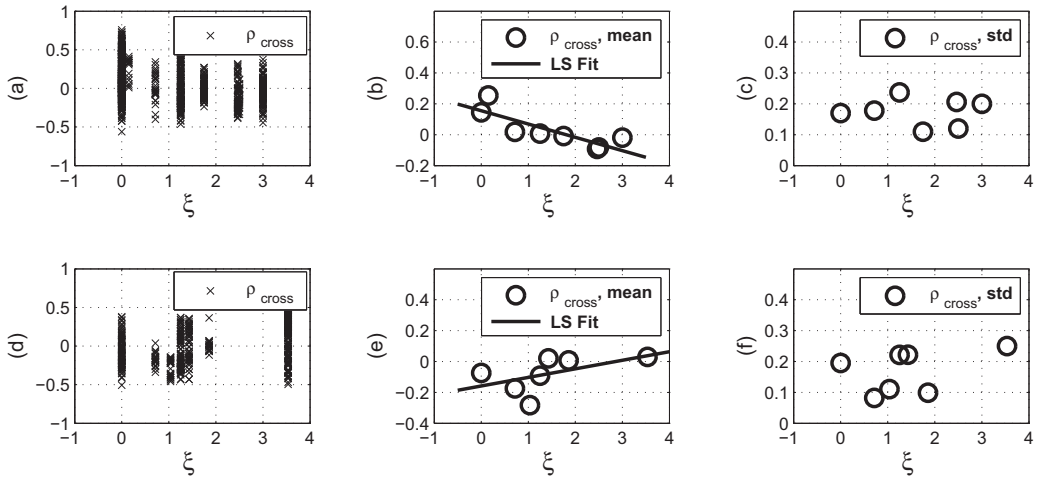

Fig. 7. Example plots of $\hat{\rho}_{\text{cross}}$. (a)-(c): Viaduct environment. (d)-(f): Cutting environment.

observation in Fig. 7(a) and (d) is that within each set of $\Phi_{j,q}$ (i.e., for each particular $\xi_{j,q}$), $\hat{\rho}_{\text{cross},j,q,p}$ generally has a large variation, and a distribution ranging between -1 and 1 should be used to describe the variation. Meanwhile, the mean value of $\hat{\rho}_{\text{cross},j,q,p}$ within the set $\Phi_{j,q}$, defined as

$$\bar{\rho}_{\text{cross},j,q} = \frac{1}{P_{j,q}} \cdot \left(\sum_{p=1}^{P_{j,q}} (\hat{\rho}_{\text{cross},j,q,p}) \right) , \qquad (12)$$

is found to follow a linear function of $\xi_{j,q}$, as shown in Fig. 7(b) and (e). It is observed that in suburban, rural, viaduct, station, and river scenarios, $\bar{\rho}_{\text{cross},j,q}$ decreases with increasing $\xi_{j,q}$; while in the cutting scenario, $\bar{\rho}_{\text{cross},j,q}$ is found to increase with $\xi_{j,q}$. Our measurements show that the cutting structure, as discussed in [22], [38], leads to a negative cross-correlation coefficient at small values of ξ. Note that in all six scenarios, a small value of $|\bar{\rho}_{\text{cross},j,q}|$ is generally observed at large $\xi_{j,q}$, which follows the physical insight that a small $\xi_{j,q}$ implies that the scenario difference[3] between the two links is small and therefore a large cross-correlation is observed. Finally, the standard deviation of $\hat{\rho}_{\text{cross},j,q,p}$ within the set $\Phi_{j,q}$, defined as

$$\sigma_{\text{cross},j,q} = \sqrt{\frac{1}{P_{j,q}} \cdot \left(\sum_{p=1}^{P_{j,q}} \left(\hat{\rho}_{\text{cross},j,q,p} - \bar{\rho}_{\text{cross},j,q}\right)^2 \right)} , \qquad (13)$$

is found to be independent of $\xi_{j,q}$, as shown in Fig. 7(c) and (f). Note that when calculating $\sigma_{\text{cross},j,q}$ in Fig. 7 and in the following analysis, we drop the sets of $\Phi_{j,q}$ where $P_{j,q} < 20$, because the size of those sets can not guarantee sufficient accuracy of standard deviation estimation. Measurements for other environments were verified, though relevant plots are not shown here due to space limitations.

Summarizing, our model of $\hat{\rho}_{\text{cross}}$ is as follows:

- We use the truncated Gaussian distribution bounded between -1 and 1 to describe the variation of $\hat{\rho}_{\text{cross},j,q,p}$ within the set of $\Phi_{j,q}$. The truncated Gaussian distribution bounded between -1 and 1 is defined as in Eq. (14), where
$$\text{erf}(x) = \frac{2}{\sqrt{\pi}} \int_0^x \exp(-t^2) dt \qquad (15)$$
is the error function.
- $\bar{\rho}_{\text{cross},j,q}$ is modeled as a linear function of $\xi_{j,q}$, expressed as
$$\bar{\rho}_{\text{cross},j,q} = a \cdot \xi_{j,q} + b \ , \qquad (16)$$
where a and b are obtained through a LS regression fit.

[3]Here the "scenario" includes the environment and BS/antenna characteristics.

This article has been accepted for publication in a future issue of this journal, but has not been fully edited. Content may change prior to final publication. Citation information: DOI 10.1109/TVT.2014.2351579, IEEE Transactions on Vehicular Technology

$$f\left(\hat{\rho}_{\mathrm{cross},j,q,p} \in \Phi_{j,q}; \bar{\rho}_{\mathrm{cross},j,q}, \sigma_{\mathrm{cross},j,q}, -1, 1\right) = \frac{\frac{1}{\sqrt{2\pi}} \exp\left(-0.5\left(\frac{\hat{\rho}_{\mathrm{cross},j,q,p} - \bar{\rho}_{\mathrm{cross},j,q}}{\sigma_{\mathrm{cross},j,q}}\right)^2\right)}{0.5\left[1 + \mathrm{erf}\left(\frac{1 - \bar{\rho}_{\mathrm{cross},j,q}}{\sqrt{2}\sigma_{\mathrm{cross},j,q}}\right)\right] - 0.5\left[1 + \mathrm{erf}\left(\frac{-1 - \bar{\rho}_{\mathrm{cross},j,q}}{\sqrt{2}\sigma_{\mathrm{cross},j,q}}\right)\right]} \tag{14}$$

TABLE VI
CROSS-CORRELATION MODEL PARAMETERS IN RAILWAY ENVIRONMENTS

Environment	a	b	$\bar{\sigma}_{\mathrm{cross}}$	RMSE
Suburban	-0.055	0.25	0.16	0.08
Rural	-0.016	0.066	0.18	0.07
Viaduct	-0.086	0.16	0.17	0.06
Cutting	0.056	-0.16	0.17	0.09
Station	-0.053	0.23	0.14	0.09
River	-0.016	0.22	0.21	0.03

- Instead of modeling $\sigma_{\mathrm{cross},j,q}$ as a function of $\xi_{j,q}$, we simply average $\sigma_{\mathrm{cross},j,q}$ in the j-th environment, expressed as

$$\bar{\sigma}_{\mathrm{cross},j} = \frac{1}{Q_j} \cdot \left(\sum_{q=1}^{Q_j} \left(\sigma_{\mathrm{cross},j,q}\right)\right) \quad . \tag{17}$$

  This is because i) no distinct dependency of $\sigma_{\mathrm{cross},j,q}$ on $\xi_{j,q}$ is observed, as shown in Fig. 7(c) and (f); and ii) Eq. (17) reduces the estimation error caused by the different $P_{j,q}$ in each set of $\Phi_{j,q}$ and avoids misleading conclusions.

In Fig. 8, we show the example CDF plots of the estimated $\hat{\rho}_{\mathrm{cross}}$ for $\xi = 0$ case in the viaduct and cutting environments. It is found that the truncated Gaussian distribution offers a reasonable fit, which has a KS passing rate larger than 87% in all six environments. The goodness-of-fit of the Uniform distribution is also examined but it generally exhibits a KS passing rate lower than 50%.

In Table VI, we summarize the obtained parameters of the cross-correlation model in Eq. (16) and (17) [4]. Note that our model is derived from the measurements conducted with a particular GSM-R system, and it is therefore limited to these conditions, e.g., the range of ξ in Table V. The root mean squared error (RMSE) of (16), as defined in [38], is calculated and summarized in Table VI. We can see that the RMSE is generally less than 0.1, which means the model has a reasonable fit.

D. Model Implementation and Validation

Since it is very difficult to conduct practical channel measurements in HSR, a recipe of the generation of the large-scale fading channel is very useful for system design. Based on the results in this paper, it is possible to model shadow fading by generating a sequence of values (in dB) that have the desired normal distribution, and possess the necessary correlation properties. We describe below the steps required to generate the shadow fading channels in HSR with the desired properties of Table III, IV, and VI [51]:

[4]Urban is not included due to the insufficient realizations.

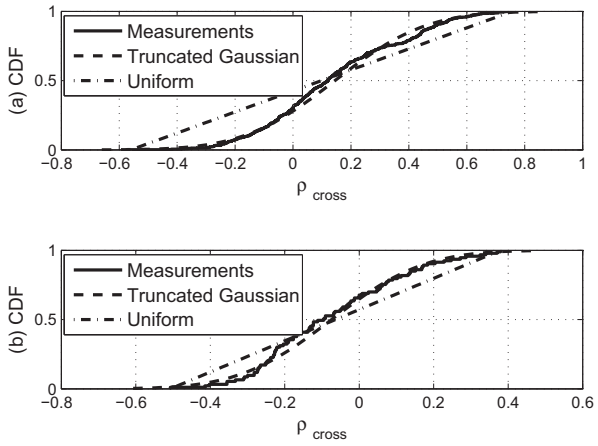

Fig. 8. Example plots of $\hat{\rho}_{\mathrm{cross}}$ when $\xi = 0$, together with the CDFs of truncated Gaussian and uniform distributions. (a) Viaduct. (b) Cutting.

1) Choose a particular environment of HSR.
2) Generate a covariance matrix $\mathbf{K}$ using the model of Eq. (9) and Table IV. Perform the following factorization: $\mathbf{K} = \mathbf{P}\Lambda\mathbf{P}^{\mathrm{T}}$, where $\mathbf{P}$ is the matrix whose columns are the eigenvectors of $\mathbf{K}$ and Λ is the diagonal matrix of eigenvalues. $(\cdot)^{\mathrm{T}}$ denotes transpose. Generating two independent identically distributed zero-mean, unit-variance Gaussian random variables x_1 and x_2. The sequences s_1 and s_2, which both have the desired covariance matrix $\mathbf{K}$, can be obtained by
$$\left[\begin{array}{cc} s_1 & s_2 \end{array}\right] = \left(\mathbf{P}\sqrt{\Lambda}\right)\left[\begin{array}{cc} x_1 & x_2 \end{array}\right] , \tag{18}$$
3) Generating two Gaussian random variables S_1 and S_2 by
$$\left[\begin{array}{cc} S_1 & S_2 \end{array}\right] = \sigma \cdot \left[\begin{array}{cc} s_1 & s_2 \end{array}\right] \cdot \mathbf{R} , \tag{19}$$
where σ is the shadow fading standard deviation in Table III. Matrix $\mathbf{R}$ is an upper triangular matrix that satisfies the equation
$$\mathbf{R}^{\mathrm{H}}\mathbf{R} = \left[\begin{array}{cc} 1 & \rho_{\mathrm{cross}} \\ \rho_{\mathrm{cross}} & 1 \end{array}\right] , \tag{20}$$
where $(\cdot)^{\mathrm{H}}$ denotes the hermitian transpose. ρ_{cross} is from the proposed model in Table VI.

This article has been accepted for publication in a future issue of this journal, but has not been fully edited. Content may change prior to final publication. Citation information: DOI 10.1109/TVT.2014.2351579, IEEE Transactions on Vehicular Technology

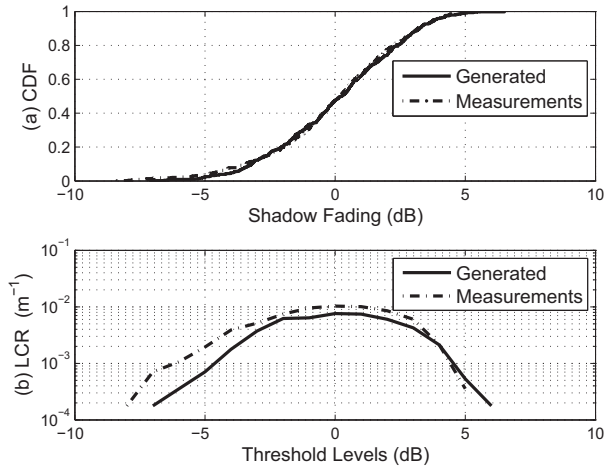

Fig. 9. Validations using the measurements of "Beijing-Shanghai" HSR in a suburban NC, where $\xi = 0$. (a) CDF. (b) LCR.

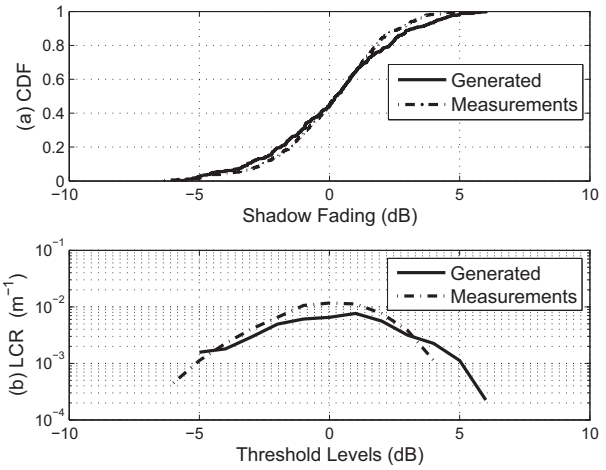

Fig. 10. Validations using the measurements of "Beijing-Shanghai" HSR in a rural NC, where $\xi = 5.83$. (a) CDF. (b) LCR.

S_1 and S_2 can thus be considered as the shadow fading components of two neighboring BSs in one NC, with the desired correlation properties.

To validate the proposed correlation model, we use the measurements from 10 cells in another HSR line, i.e. the "Beijing-Shanghai" line, whose measurements were not used in the development of the above models. The measurement system is the same as reported in Section III. We generate the shadow fading components with the same number of samples to the measurements. The generated sequences of shadow fading, with full auto- and cross-correlation properties, are compared with the measurements in "Beijing-Shanghai" line, and both first- and second-order statistics are validated as follows.

1) First-Order Statistics Validation: We compare the CDF of the generated shadow fading components with measurements. Examples of CDF comparisons in suburban and rural environments are presented in Fig. 9(a) and Fig. 10(a), where we can see that the generated sequences offer a reasonable fit to the measurements.

2) Second-Order Statistics Validation: We use the level crossing rate (LCR) of the shadow fading to validate the second-order statistics of our model. The LCR is defined as the number of times that the signal crosses a given threshold level from up to down within a unit of length (1 m) [52]. Examples of LCR comparisons in suburban and rural environments are presented in Fig. 9(b) and Fig. 10(b). We find the LCRs of the generated shadow fading to be fairly close to the measurements in both cases. Measurements for other environments were also verified, though relevant plots are not shown here due to space limitations.

VI. Conclusion

To develop new and better handover schemes for HSR, a deep understanding of the correlation properties of the shadow fading is required. In this paper, we have presented a comprehensive analysis and modeling of shadow fading in HSR environments. The work is based on a large experimental dataset with 6146 cells along the HSR lines of China, using an operative GSM-R system at 930 MHz. The measurements were conducted in 7 typical HSR environments. For each environment, we analyze both auto- and cross-correlation properties of shadow fading. It is found that the decorrelation distance is correlated with the standard deviation of shadow fading and is generally larger than 100 m in most HSR environments. The cross-correlation of shadow fading between two neighboring BSs depends upon the BS height and the tilt angle of the antenna. A truncated Gaussian distribution is found to fit the variation of cross-correlation coefficient reasonably, and a heuristic model is then proposed. The model is validated by measurements conducted in another HSR line. The results in this paper can be used to exploit the simulation algorithms, to analyze the signal-to-interference-ratio (SIR) properties, and to develop the new and better handover schemes for HSRs.

References

[1] R. He, Z. Zhong, B. Ai, and B. Zhang, "Measurement-based auto-correlation model of shadow fading for the high-speed railways in urban, suburban, and rural environments," *Proc. IEEE APS'14*, pp. 1–2, Memphis, USA, Jul. 2014.

[2] R. He, Z. Zhong, B. Ai, and C. Oestges, "A heuristic cross-correlation model of shadow fading in high-speed railway environments," *Proc. URSI GASS'14*, pp. 1–4, Beijing, China, Aug. 2014.

[3] "Mid- and Long-Term Plan of Railway Networks," [Online]. Available: http://baike.baidu.com/view/1463367.htm.

[4] W. C. Jakes and D. C. Cox, *Microwave mobile communications*. Wiley-IEEE Press, 1994.

[5] R. C. Bernhardt, "Macroscopic diversity in frequency reuse radio systems," *IEEE J. Sel. Areas Commun.*, vol. 5, no. 5, pp. 862–870, 1987.

[6] E. Perahia, D. C. Cox, and S. Ho, "Shadow fading cross correlation between basestations," in *Proc. IEEE VTC'01*, Rhodes, Greece, May 2001, pp. 313–317.

[7] G. L. Stüber, *Principles of mobile communication*. Springer, 2011.

[8] B. Singh, K. Aggarwal, and S. Kumar, "Sensitivity analysis of handover performance to shadow fading in microcellular systems," in *Proc. IEEE ICPWC'05*, New Delhi, India, Jan. 2005, pp. 446–450.

[9] L. Tian, J. Li, Y. Huang, J. Shi, and J. Zhou, "Seamless dual-link handover scheme in broadband wireless communication systems for high-speed rail," *IEEE J. Sel. Areas Commun.*, vol. 30, no. 4, pp. 708–718, 2012.

[10] N. Benvenuto and F. Santucci, "A least squares path-loss estimation approach to handover algorithms," *IEEE Trans. Veh. Technol.*, vol. 48, no. 2, pp. 437–447, 1999.

[11] M. Gudmundson, "Analysis of handover algorithms," in *Proc. IEEE VTC'91*, St. Louis, USA, May 1991, pp. 537–542.

[12] K. Kumaran, S. E. Golowich, and S. Borst, "Correlated shadow-fading in wireless networks and its effect on call dropping," *Wireless networks*, vol. 8, no. 1, pp. 61–71, 2002.

[13] F. Graziosi, M. Pratesi, M. Ruggieri, and F. Santucci, "A multicell model of handover initiation in mobile cellular networks," *IEEE Trans. Veh. Technol.*, vol. 48, no. 3, pp. 802–814, 1999.

[14] H.-P. Lin, R.-T. Juang, and D.-B. Lin, "Validation of an improved location-based handover algorithm using GSM measurement data," *IEEE Trans. Mobile Comput.*, vol. 4, no. 5, pp. 530–536, 2005.

[15] J. Meinilä, P. Kyösti, T. Jämsä, and L. Hentilä, "WINNER II channel models," *Radio Technologies and Concepts for IMT-Advanced*, pp. 39–92, 2009.

[16] H. Wei, Z. Zhong, L. Xiong, B. Ai, and R. He, "Study on the shadow fading characteristic in viaduct scenario of the high-speed railway," in *Proc. IEEE CHINACOM'11*, Harbin, China, Aug. 2011, pp. 1216–1220.

[17] Y. Guo, J. Zhang, C. Zhang, and L. Tian, "Correlation analysis of high-speed railway channel parameters based on channel measurement," in *Proc. IEEE HMWC'13*, Shanghai, China, Nov. 2013, pp. 132–136.

[18] R. He, Z. Zhong, and B. Ai, "Path loss measurements and analysis for high-speed railway viaduct scene," in *Proc. IWCMC'10*, Caen, France, July 2010, pp. 266–270.

[19] L. Liu, C. Tao, J. Qiu, H. Chen, L. Yu, W. Dong, and Y. Yuan, "Position-based modeling for wireless channel on high-speed railway under a viaduct at 2.35 GHz," *IEEE J. Sel. Areas Commun.*, vol. 30, no. 4, pp. 834–845, 2012.

[20] Y. Guo, J. Zhang, C. Tao, L. Liu, and L. Tian, "Propagation characteristics of wideband high-speed railway channel in viaduct scenario at 2.35 GHz," *J. Modern Transp.*, vol. 20, no. 4, pp. 206–212, 2012.

[21] M. Zhao, M. Wu, Y. Sun, G. Jia, S. Di, P. Zhou, X. Zeng, and S. Ge, "Analysis and modeling of the LTE broadband channel for train-ground communications on high-speed railway," in *Proc. IEEE VTC'13*, Las Vegas, USA, Sept. 2013, pp. 1–5.

[22] R. He, Z. Zhong, B. Ai, and J. Ding, "Propagation measurements and analysis for high-speed railway cutting scenario," *Electron. Lett.*, vol. 47, no. 21, pp. 1167–1168, 2011.

[23] R. Sun, C. Tao, L. Liu, and Z. Tan, "Channel measurement and characterization for HSR U-shape groove scenarios at 2.35 GHz," in *Proc. IEEE VTC'13*, Las Vegas, USA, Sept. 2013, pp. 1–5.

[24] F. Luan, Y. Zhang, L. Xiao, C. Zhou, and S. Zhou, "Fading characteristics of wireless channel on high-speed railway in hilly terrain scenario," *Int. J. Antennas Propag.*, vol. 2013, 2013.

[25] C. R. Garcia, A. Lehner, T. Strang, and K. Frank, "Channel model for train to train communication using the 400 MHz band," in *Proc. IEEE VTC'08*, Singapore, May 2008, pp. 3082–3086.

[26] F. Abrishamkar and J. Irvine, "Comparison of current solutions for the provision of voice services to passengers on high speed trains," in *Proc. IEEE VTC'00*, vol. 5, Boston, USA, Sept. 2000, pp. 2068–2075.

[27] Y. Zhang, Z. He, W. Zhang, L. Xiao, and S. Zhou, "Measurement-based delay and Doppler characterizations for high-speed railway hilly scenario," *Int. J. Antennas Propag.*, vol. 2014, 2014.

[28] T. Zhou, C. Tao, L. Liu, J. Qiu, and R. Sun, "High-speed railway channel measurements and characterizations: a review," *J. Modern Transp.*, vol. 20, no. 4, pp. 199–205, 2012.

[29] M. Gudmundson, "Correlation model for shadow fading in mobile radio systems," *Electron. lett.*, vol. 27, no. 23, pp. 2145–2146, 1991.

[30] Y. Zhang, J. Zhang, D. Dong, X. Nie, G. Liu, and P. Zhang, "A novel spatial autocorrelation model of shadow fading in urban macro environments," in *Proc. IEEE GLOBECOM'08*, New Orleans, USA, Dec. 2008, pp. 1–5.

[31] A. Algans, K. I. Pedersen, and P. E. Mogensen, "Experimental analysis of the joint statistical properties of azimuth spread, delay spread, and shadow fading," *IEEE J. Sel. Areas Commun.*, vol. 20, no. 3, pp. 523–531, 2002.

[32] T. Sorensen, "Slow fading cross-correlation against azimuth separation of base stations," *Electron. Lett.*, vol. 35, no. 2, pp. 127–129, 1999.

[33] J. Weitzen and T. J. Lowe, "Measurement of angular and distance correlation properties of log-normal shadowing at 1900 MHz and its application to design of PCS systems," *IEEE Trans. Veh. Technol.*, vol. 51, no. 2, pp. 265–273, 2002.

[34] M. Zhu, F. Tufvesson, and J. Medbo, "Correlation properties of large scale parameters from 2.66 GHz multi-site macro cell measurements," in *Proc. IEEE VTC'11*, Budapest, Hungary, May 2011, pp. 1–5.

[35] Q. H. Chu, J.-M. Conrat, and J. Cousin, "Experimental characterization and modeling of shadow fading correlation for relaying systems," in *Proc. IEEE VTC'11*, San Francisco, USA, Sept. 2011, pp. 1–5.

[36] S. S. Szyszkowicz, H. Yanikomeroglu, and J. S. Thompson, "On the feasibility of wireless shadowing correlation models," *IEEE Trans. Veh. Technol.*, vol. 59, no. 9, pp. 4222–4236, 2010.

[37] R. He, Z. Zhong, B. Ai, G. Wang, J. Ding, and A. Molisch, "Measurements and analysis of propagation channels in high-speed railway viaducts," *IEEE Trans. Wireless Commun.*, vol. 12, no. 2, pp. 794–805, 2013.

[38] R. He, Z. Zhong, B. Ai, J. Ding, Y. Yang, and A. Molisch, "Short-term fading behavior in high-speed railway cutting scenario: Measurements, analysis, and statistical models," *IEEE Trans. Antennas Propag.*, vol. 61, no. 4, pp. 2209–2222, 2013.

[39] R. He, Z. Zhong, B. Ai, and J. Ding, "An empirical path loss model and fading analysis for high-speed railway viaduct scenarios," *IEEE Antennas Wireless Propag. Lett.*, vol. 10, pp. 808–812, 2011.

[40] B. Ai, R. He, Z. Zhong, K. Guan, B. Chen, P. Liu, and Y. Li, "Radio wave propagation scene partitioning for high-speed rails," *Int. J. Antennas Propag.*, vol. 2012, 2012.

[41] R. He, Z. Zhong, B. Ai, J. Ding, W. Jiang, H. Zhang, and X. Li, "A standardized path loss model for the GSM-railway based high-speed railway communication systems," in *Proc. IEEE VTC'14*, Seoul, Korea, May 2014, pp. 1–5.

[42] A. F. Molisch, *Wireless communications*. Wiley, 2010.

[43] R. A. Fisher *et al.*, "Frequency distribution of the values of the correlation coefficient in samples from an indefinitely large population," *Biometrika*, vol. 10, no. 4, pp. 507–521, 1915.

[44] D. G. Altman and M. J. Gardner, "Statistics in medicine: Calculating confidence intervals for regression and correlation," *British Medical Journal*, vol. 296, no. 6631, pp. 1238–1242, 1988.

[45] C. Walck, "Handbook on statistical distributions for experimentalists," 2007.

[46] F. J. Massey Jr, "The Kolmogorov-Smirnov test for goodness of fit," *J. American statistical Association*, vol. 46, no. 253, pp. 68–78, 1951.

[47] V. Erceg, L. J. Greenstein, S. Y. Tjandra, S. R. Parkoff, A. Gupta, B. Kulic, A. A. Julius, and R. Bianchi, "An empirically based path loss model for wireless channels in suburban environments," *IEEE J. Sel. Areas Commun.*, vol. 17, no. 7, pp. 1205–1211, 1999.

[48] J. Fischer, M. Grossmann, W. Felber, M. Landmann, and A. Heuberger, "Modeling shadow fading for mobile-to-mobile communications in the VHF and UHF band," in *Proc. IEEE ICWITS'12*, Hawaii, USA, Nov. 2012, pp. 1–4.

[49] R. He, A. F. Molisch, Z. Zhong, B. Ai, J. Ding, R. Chen, and Z. Li, "Measurement based channel modeling with directional antennas for high-speed railways," in *Proc. IEEE WCNC'13*, Shanghai, China, April 2013, pp. 2932–2936.

[50] R. He, Z. Zhong, B. Ai, and J. Ding, "Measurements and analysis of the directional antenna bottom area in high speed rail," in *Proc. IEEE APS'12*, Chicago, USA, July 2012, pp. 1–2.

[51] A. Leon-Garcia, *Probability, Statistics, and Random Processes For Electrical Engineering*. Pearson Prentice Hall, 2008, ch. 6 and 10.

[52] M. Pätzold and K. Yang, "An exact solution for the level-crossing rate of shadow fading processes modelled by using the sum-of-sinusoids principle," *Wireless Pers. Commun.*, vol. 52, no. 1, pp. 57–68, 2010.

This article has been accepted for publication in a future issue of this journal, but has not been fully edited. Content may change prior to final publication. Citation information: DOI 10.1109/TVT.2014.2351579, IEEE Transactions on Vehicular Technology

Ruisi He (S'11-M'13) received B.E. degree from Beijing Jiaotong University in 2009. Currently, he is working toward the Ph.D. degree in State Key Laboratory of Rail Traffic Control and Safety & School of Electronic and Information Engineering, Beijing Jiaotong University. He has also been a research assistant of State Key Laboratory of Rail Traffic Control and Safety since 2014. From Mar. to Sept. 2010, he has been a visiting scholar in Universidad Politécnica de Madrid, Spain. From Aug. 2012 to Sept. 2013, he has been a research scholar at the Department of Electrical and Engineering, University of Southern California, Los Angeles, USA. From Dec. 2013 to Jul. 2014, he has been a visiting scholar at the Institute for Information and Communication Technologies, Université Catholique de Louvain, Belgium. Mr. He's current research interests are measurement and modeling of wireless propagation channels, high-speed railway and vehicular communications, antennas, and signal processing. Mr. He has authored/co-authored over 40 research papers in international journals and conferences.

Mr. He serves as the Early Career Representative (ECR) of Commission C - Radiocommunication Systems and Signal Processing, International Union of Radio Science (URSI), from 2014-2017. He serves as a Technical Program Committee (TPC) chair of "Antenna and wave propagation" for APEMC 2015, and as a TPC member for the IEEE ICC 2015, GLOBECOM 2014, VTC 2014, and IWCMC 2014. He is also assigned as a section editor of the section "railway communications" for the upcoming COST IC1004 final book. He received the Best Paper Award in IEEE ICGSIS in 2011, the IBM Excellent Student Award of China in 2013, and Siemens Scholarship in 2012. He is a member of the IEEE and a member of the COST IC1004.

Zhangdui Zhong is a professor and advisor of Ph.D. candidates in Beijing Jiaotong University. He is now a director of School of Computer and Information Technology and a Chief Scientist of State Key Laboratory of Rail Traffic Control and Safety in Beijing Jiaotong University. He is also a director of the Innovative Research Team of Ministry of Education, and a Chief Scientist of Ministry of Railways in China. He is an executive council member of Radio Association of China, and a deputy director of Radio Association of Beijing. His interests are wireless communications for railways, control theory and techniques for railways, and GSM-R system. His research has been widely used in the railway engineering, such as Qinghai-Xizang railway, Datong-Qinhuangdao Heavy Haul railway, and many high-speed railway lines of China.

He has authored/co-authored 7 books, 5 invention patents, and over 200 scientific research papers in his research area. He received MaoYiSheng Scientific Award of China, ZhanTianYou Railway Honorary Award of China, and Top 10 Science/Technology Achievements Award of Chinese Universities.

Bo Ai (M'00-SM'10) received his Master and Ph.D. degree from Xidian University in 2002 and 2004 in China, respectively. He graduated in 2007 with great honors of Excellent Postdoctoral Research Fellow in Tsinghua University. He is now working in Beijing Jiaotong University as a professor and advisor of Ph.D. candidates. He is a deputy director of State Key Laboratory of Rail Traffic Control and Safety. He is an associate editor for IEEE Trans. on Consumer Electronics and an editorial committee member of journal of Wireless Personal Communications. He has authored/co-authored 6 books, 26 invention patents and 130 scientific research papers in his research area till now. His current interests are the research and applications OFDM techniques, HPA linearization techniques, radio propagation and channel modeling, GSM Railway systems. He is an IET Fellow, an IEEE Senior member, and a senior member of Electronics Institute of China (CIE).

Claude Oestges (M'05-SM'12) received the M.Sc. and Ph.D. degrees in Electrical Engineering from the Université catholique de Louvain (UCL), Louvain-la-Neuve, Belgium, respectively in 1996 and 2000. In January 2001, he joined as a post-doctoral scholar the Smart Antennas Research Group (Information Systems Laboratory), Stanford University, CA, USA. From January 2002 to September 2005, he was associated with the Microwave Laboratory UCL as a post-doctoral fellow of the Belgian Fonds de la Recherche Scientifique (FRS-FNRS). Claude Oestges is presently Associate Professor with the Electrical Engineering Department, Institute for Information and Communication Technologies, Electronics and Applied Mathematics, UCL. He also currently serves as an Associate Editor for the IEEE Transactions on Antennas and Propagation and the IEEE Transactions on Vehicular Technology. He is the author or co-author of three books and more than 180 journal papers and conference communications, and was the recipient of the 1999-2000 IET Marconi Premium Award and of the IEEE Vehicular Technology Society Neal Shepherd Award in 2004 and 2012.